Available online at www.sciencedirect.com
ScienceDirect
Journal of the European Ceramic Society 28 (2008) 779–785
www.elsevier.com/locate/jeurceramsoc

The influence of screen-printing parameters on the microstructure and gas permeance of a zirconia electrolyte

Gary J. Wright [a,b,*], Julie A. Yeomans [a]

[a] *School of Engineering, University of Surrey, Guildford, Surrey GU2 7XH, UK*
[b] *Rolls-Royce Fuel Cell Systems Ltd., Loughborough, Leicestershire LE11 3GR, UK*

Received 27 May 2007; received in revised form 24 August 2007; accepted 1 September 2007
Available online 22 October 2007

Abstract

Yttria-stabilised zirconia (YSZ) was screen-printed onto the surface of porous pre-fired substrates using different mesh thicknesses. As deposited layer thickness increased from 46 to 310 μm, the resultant sintered layer thickness increased from 3 to 17 μm, resulting in a reduction in grain size from 2.2 to 0.9 μm and relative density from 0.94 to 0.81. The gas permeance through the constrained sintered film was measured and the lowest gas permeance of 1.3×10^{-4} mbar l s^{-1} cm^{-2} was recorded for a layer with a thickness of 9 μm, indicating that a number of parameters need to be considered together to achieve the optimum microstructure.

Keywords: Sintering; Grain size; ZrO_2; Fuel cells

1. Introduction

Yttria-stabilised zirconia (YSZ) is used in a range of industrial applications, including gas sensors, solid oxide fuel cells (SOFCs), catalytic membranes and thermal barrier coatings, due to its unique combination of properties such as high chemical and thermal stability and ionic conductivity over a wide range of temperatures.[1] SOFCs are being actively developed as a means of power generation.[2,3] The sintered layer thickness requirement for a typical thick-film electrolyte is ~10–20 μm,[4] but recent developments have focussed on YSZ electrolytes of ≤10 μm[5] with an emphasis on reducing the polarisation effects of the layer.[6] Thick-film technology, such as screen-printing, offers the prospect of lower-cost SOFC fabrication; however, the printing, drying and firing of constrained thick-films is difficult.[7]

Screen-printing is of interest as it is a process designed for the production of consistent layers. Although the development of inks specific to SOFCs is a relatively routine process, at the laboratory level, good controls of the ink rheology, screen-printing parameters, drying and sintering processes are vital for the attainment of a body of sufficient quality for a SOFC electrolyte.[8] Within the screen-printing process a number of parameters can be controlled, including screen thickness (mesh size), print gap, printing speed and squeegee pressure. Application of the thick-film to a pre-sintered substrate results in the electrolyte sintering under constraint.

Constrained sintering can retard densification,[9] resulting in porosity and where this is open, i.e. interconnected, this would be detrimental in gas sensor or SOFC applications,[8] since a chief requirement is that the layer be impermeable to the gases of interest.

Several investigations have found that porous low density microstructures are inherent in the screen-printing process.[8,10] However, changes in the thickness of the screen, denoted by the size of the wires that create the mesh, result in different sintered microstructures and these in turn change the gas permeance of the film.[11] Gaudon et al.,[12] observed that the gas permeance of constrained YSZ films was influenced by the density of the green body. However, Park et al.,[13] reported that the major influence on gas permeance was the ratio between the pre-fired substrate pore size and the sintered layer thickness.[13] Nano-porous substrates were coated with nanometre thick layers. The gas permeance was minimised for a substrate pore size of 20 nm and layer thickness of 35 nm. Increasing the substrate pore size and layer thickness subsequently increased the gas permeance.

* Corresponding author. Tel.: +44 1509 225443; fax: +44 1509 225501.
E-mail address: gary.wright@rrfcs.com (G.J. Wright).

0955-2219/$ – see front matter © 2007 Elsevier Ltd. All rights reserved.
doi:10.1016/j.jeurceramsoc.2007.09.027

All of the previous studies were concerned with gas permeance of layers sintered on pre-fired substrates. Whilst providing useful insights into the rate of gas loss across the constrained sintered film, these studies do not provide detailed microstructural information relating to the sintered films themselves. As the gas permeance is a function of the microstructure, parameters such as sintered layer thickness, relative density and grain size of constrained YSZ layers are examined in the present study.

2. Experimental procedure

2.1. Sample preparation

A square pattern YSZ layer was screen-printed using a SMTECH Benchmark 90 screen printer, on 50 mm × 50 mm pre-fired porous magnesia-rich spinel substrates (Advanced Ceramics Ltd., UK). A priming layer consisting of YSZ was deposited onto the substrate at a thickness of ∼30 μm. The priming layer was pre-fired prior to the application of the YSZ thick-film to reduce the surface roughness of the sintered substrate as shown in Fig. 1. Mesh screens (MCI Cambridge Ltd., UK) of increasing thickness were used ranging from 325 apertures per inch (API) (∼60 μm) to 80 API (∼215 μm). As the ink passes across the screen, only the open areas within the mesh are available for the ink to flow through. Therefore, the volume of ink deposited through the screen is a function of the screen thickness and open area of the mesh. This reduces the thickness of the printed (wet) and dried layer relative to the screen thickness. Additional print-dry applications prior to sintering increases the sintered layer thickness,[11] but in this study three print-dry applications were used throughout.

Details of the samples that were fabricated with different mesh size, screen thickness and print-dry applications are given in Table 1. All other parameters, e.g. squeegee pressure, printing speed were kept constant. The YSZ ink consisted of 50 wt.% solids loading of 3 mol% YSZ powder (MEL Chemicals, UK) mixed with 63/2 Medium, a terpineol based binder (Johnson Matthey, UK) with a single batch of ink used throughout the study. A sample index was adopted which identifies the mesh size and number of print-dry applications applied to the sample. A sample screen-printed with a 325-mesh size and three print-dry deposits would be assigned the sample identification 325-3.

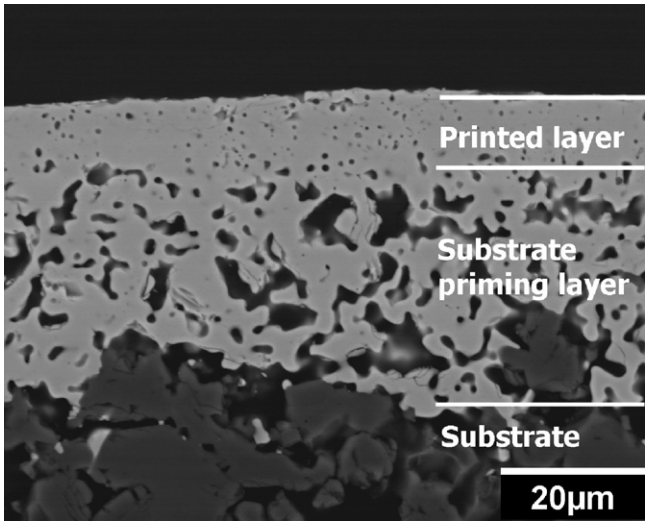

Fig. 1. Scanning electron micrograph of cross-section of a typical sintered screen-printed layer showing the pre-fired substrate priming layer and substrate.

Table 1
Details of samples printed using increasing screen thickness

Sample no.	Number of print-dry applications	Mesh size (API)	Screen thickness (μm)
325-3	3	325	60
200-3	3	200	90
165-3	3	165	110
105-3	3	105	162
80-3	3	80	215

The samples were all dried at 80 °C for 30 min after each print-dry application, prior to the sintering stage. A heating rate of 3 °C min^{-1}, sintering temperature of 1450 °C and dwell time of 1 h, all in an air atmosphere, was the sintering cycle used throughout this study.

2.2. Gas permeance measurement

The amount of gas leakage across the sintered films was characterised by gas flow rate measurements. The room temperature method essentially compares the inlet flow with the outlet flow resulting in a measured gas flow rate of helium that is lost through the sintered film. The gas test uses a 2 l min^{-1} (hydrogen) mass flow controller supplied by Bronkhurst (High-tech, EL-flow) on the sample inlet and mass flow meter on the exhaust. Each sample was analysed using 100% helium supplied by BOC (Derby, UK). Each sample was analysed using an inlet flow rate of 1 l min^{-1} and the total outlet flow rate was measured by the mass flow meter. The flow in the outlet or exhaust is relative to the flow controller reading at the inlet as a function of the flow meter reading at the outlet. Therefore, the helium flow rate in millilitre per min out of the sample is used to calculate the gas permeance defined as:

$$\text{gas permeance} = \left(\frac{\text{flow rate}}{\text{area}}\right)\Delta P \quad (1)$$

where flow rate is the flow in the exhaust as a ratio of the inlet and outlet flow meter readings, area the thick-film surface exposed to the test gas and ΔP is the differential pressure across the thick-film.

Mean gas permeance values were calculated from measurements on at least five samples for each fabrication method to reduce the potential errors associated with the porous substrate and fabrication of the screen-printed layers.

2.3. Microstructural characterisation

Microstructural characterisation was performed using scanning electron microscopy (SEM, Cambridge Stereoscan 240) on surfaces and polished cross-sections. Cross sections of the samples were prepared and polished down to a 1 μm diamond

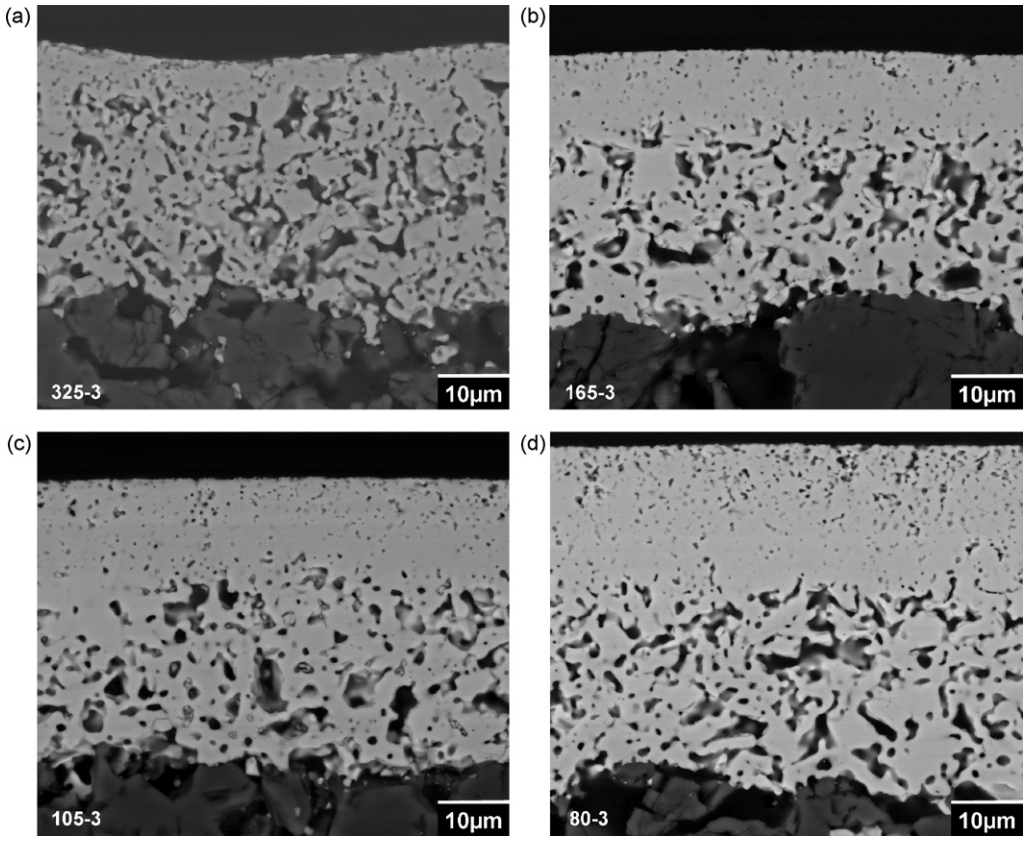

Fig. 2. Scanning electron micrographs of cross-sections of sintered layers with three print-dry applications deposited through the (a) 325, (b) 165, (c) 105 and (d) 80 mesh sizes.

paste and relief polished with a 0.04 μm colloidal silica solution (Struers, Denmark). Grain size analysis was conducted using a linear intercept technique complying with the British Standard BS EN 623-3:2001. The British standard requires at least five randomly positioned and randomly orientated lines across the micrograph such that at least 100 discrete phase regions or pores of the type to be assessed are intersected. Grains touching the edge of the micrograph are ignored and each measurement is taken to the nearest 0.5 mm with a calibrated rule. This method was also used to measure the pore size and relative density from images of the planar surfaces taken using an SEM.

Relative density of the surface can be determined by using the pore size measurements and taking the summation of all the lines measured, thus providing the proportion of open area. Variation of the layer thickness was measured using an SEM. For each test specimen five measurements per image and three images per sample were taken to determine the mean.

3. Results and discussion

3.1. Deposited and sintered thickness of screen-printed layers

The screen-printing process uses screen thickness (mesh size) to change the thickness of the laminate prior to sintering. The printing trials for each screen thickness included print-dry applications of three layers. Once fabricated, the samples were sintered once using an identical sintering profile for each batch of samples.

The effect of screen thickness on the sintered layer is shown in Fig. 2. These images show the increasing sintered layer thickness produced from samples with three print-dry applications

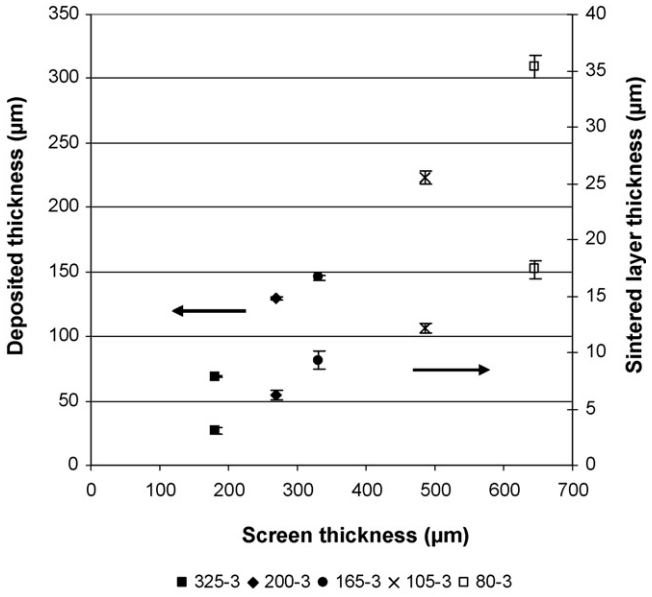

Fig. 3. Deposited thickness and sintered thickness as a function of screen thickness. Error bars represent 1S.D. from the mean.

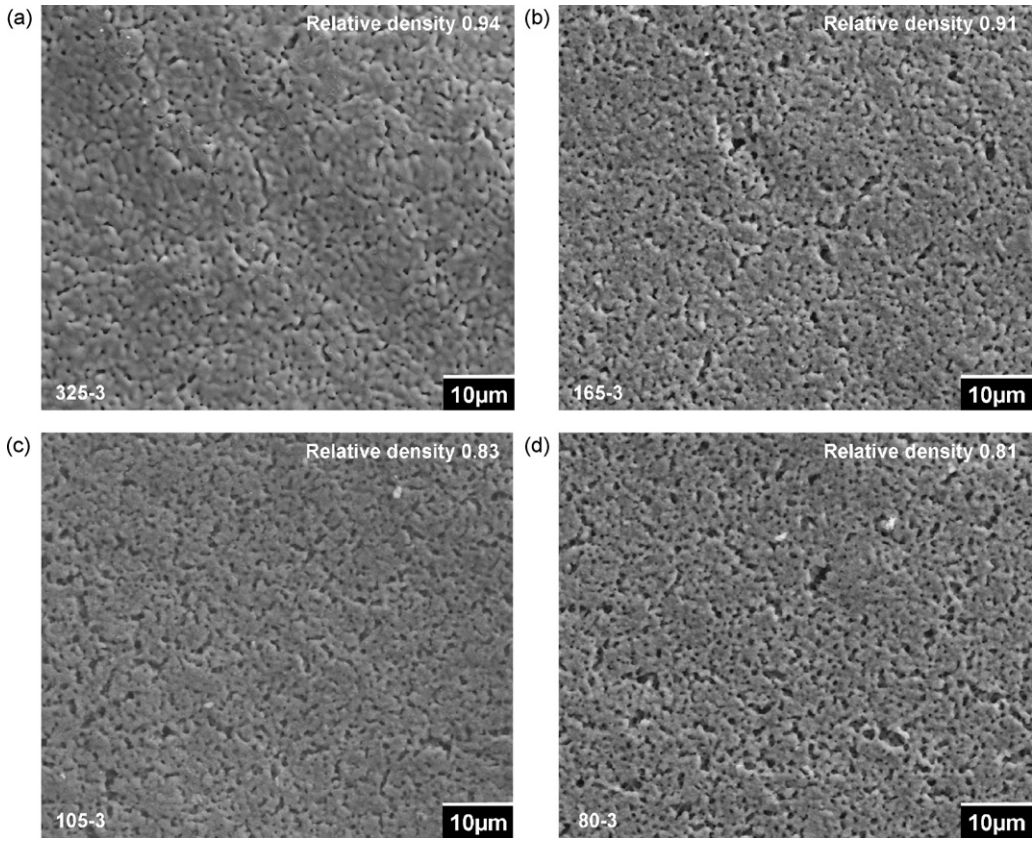

Fig. 4. Scanning electron micrographs of the surfaces of the sintered layers for (a) 325, (b) 165, (c) 105 and (d) 80 mesh sizes.

through the 325, 165, 105 and 80 mesh sizes. A microstructural examination of the cross-sections showed increasing sintered layer thickness for increasing screen thickness, as would be expected. For example, a 325-mesh size resulted in an equivalent screen thickness of 180 μm, a deposited thickness of 69 μm and sintered layer thickness of 3.0 ± 0.3 μm. At the other end of the scale, an 80-mesh size resulted in an equivalent screen thickness of 645 μm, a deposited thickness of 310 μm and sintered layer thickness of 17.0 ± 1.2 μm, as shown in Fig. 3. There would appear to be a constant ratio of deposited thickness to sintered thickness for this set of mesh sizes, of ∼18:1, indicating very large shrinkage in the vertical direction during drying and sintering.

3.2. Microstructural change with deposition thickness

Microscopy of the sintered layers showed a variation in the surface structure for increasing screen thickness. The variation in surface microstructure between samples 325-3, 165-3, 105-3 and 80-3 is presented in Fig. 4. These surface images show that sample 325-3 results in a larger grain size and reduced surface porosity when compared with samples 165-3, 105-3 and 80-3. In each case the samples were sintered using the same sintering scheme.

The relative density and grain size of the sintered layer surfaces are presented in Fig. 5. These data show that increasing the thickness of the printed layer reduces the relative density and the grain size as assessed from observation of the microstructure of the surface. For example, sample 325-3 had a relative density of 0.94 and a grain size of 2.2 ± 0.3 μm. For sample 80-3 sintered using the same sintering scheme, the relative density and grain size reduced to 0.81 and 0.94 ± 0.1 μm, respectively. The observed reduction in relative density shows an approximately

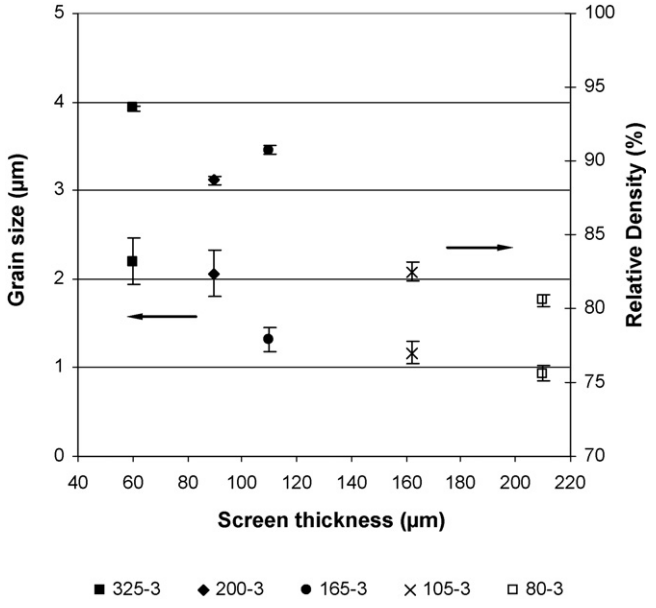

Fig. 5. The grain size and relative density as a function of increasing screen thickness. Error bars represent 1S.D. from the mean.

linear relationship with increasing screen thickness, whilst the grain size data show a less linear response.

The change in grain size for the 165, 105 and 80 mesh sizes is small compared with the change between the mesh sizes 325 and 200. Indeed, the non-parametric two-selection Wilcoxon signed-rank test[14] showed that the mean grain sizes for the 165, 105 and 80 mesh samples were not significantly different.[15] This suggests that once the screen thickness is $\geq 110\,\mu m$ the grain size remains relatively unchanged with increasing screen thickness. The general trend of these results is as expected in that the stresses arising from constraint are higher in thicker layers and thus the retardation of the densification would be expected to be greater. Likewise, grain growth is a function of relative density so it is also expected that larger grains would be found in the higher density, thinner layers.

3.3. Gas permeance of screen-printed layers

The screen-printing process can be used to produce films of increasing sintered thickness through increasing the volume of ink deposited using more print applications or different mesh sizes. The effect of pressure on gas permeance through such thick-films was measured for each mesh size and the results are shown in Fig. 6. Samples fabricated using the 325-mesh (squares) had the largest pressure dependence. This sample also had the lowest sintered thickness. Pressure had the least effect on the samples printed using the 165-mesh size (circles).

The dependence of gas permeance on layer thickness is shown more clearly in Fig. 7. The values shown are plotted for a fixed pressure of 30 mbar. A 325-mesh size with three print-dry deposits results in a gas permeance of $2.7 \times 10^{-4} \pm 7.4 \times 10^{-6}\,mbar\,l\,s^{-1}\,cm^{-2}$ and this was reduced to $1.3 \times 10^{-4} \pm 2.0 \times 10^{-5}\,mbar\,l\,s^{-1}\,cm^{-2}$ with a 165-mesh size. This value is one order of magnitude higher than that reported by Gaudon et al. where it was suggested that a thick-film electrolyte with a gas permeance value of $10^{-5}\,l\,s^{-1}\,cm^{-2}$ was suitable for use in an industrial application. Gaudon et al. achieved this value with a sintered layer thickness of $\sim 5\,\mu m$. In this study the lowest gas permeance is associated with a layer that has values of thickness, relative density and grain size, which are in the middle of the ranges evaluated, suggesting that gas permeance depends on a number of interrelated parameters.

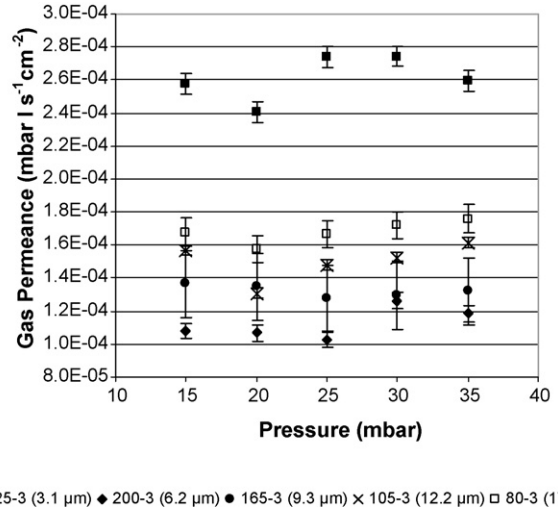

Fig. 6. Gas permeance as a function of pressure for sintered thicknesses of 3.1, 6.2, 9.3, 12.2 and 17.3 μm achieved using applications through the 325, 200, 165, 105 and 80 mesh sizes, respectively. Error bars represent 1S.D. from the mean.

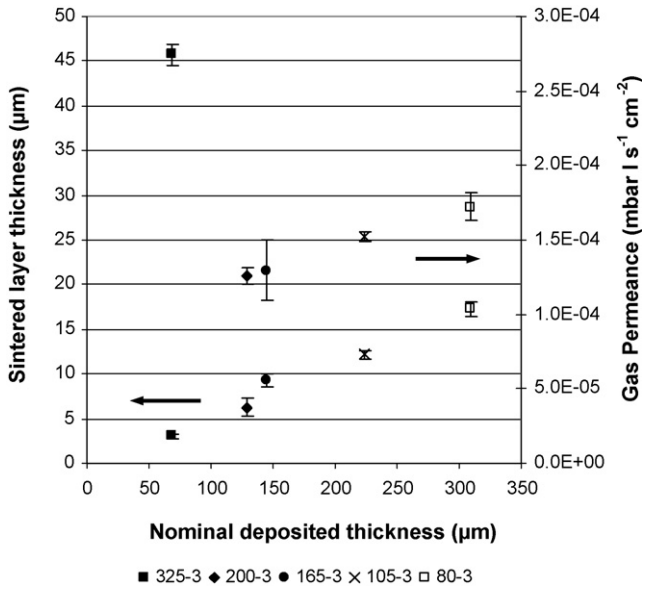

Fig. 7. Sintered layer thickness and gas permeance as a function of deposition thickness. Gas permeance values are quoted at a pressure of 30 mbar. Error bars represent 1S.D. from the mean.

3.4. Relationship between microstructural parameters and gas permeance

From the results shown in Fig. 7, it is clear that layer thickness and density are not the sole controlling factors for gas permeance. This led to a consideration of grain size. If the grain size exceeds the sintered layer thickness a potential gas flow path exists through pores and along grain boundaries. The flow path would be extended if the layer was more than one grain thick. This could in turn reduce the rate of gas permeance across the sintered layer. Gas permeance could also be reduced if the pore or grain boundaries were not aligned but offset, like bricks in a wall. The ratio, z, between the mean grain size and the sintered layer thickness can be expressed as:

$$z = \frac{\text{mean grain size}}{\text{sintered layer thickness}} \tag{2}$$

The relationship between mean grain size and the sintered layer thickness can be represented schematically as shown in Fig. 8.

When the mean grain size is only one tenth of the sintered layer then the factor z will be equal to 0.1. However, during densification the mean grain size increases and the layer thickness reduces until z becomes equal to 1. As further thermal processing occurs the surface grain size continues to increase. When

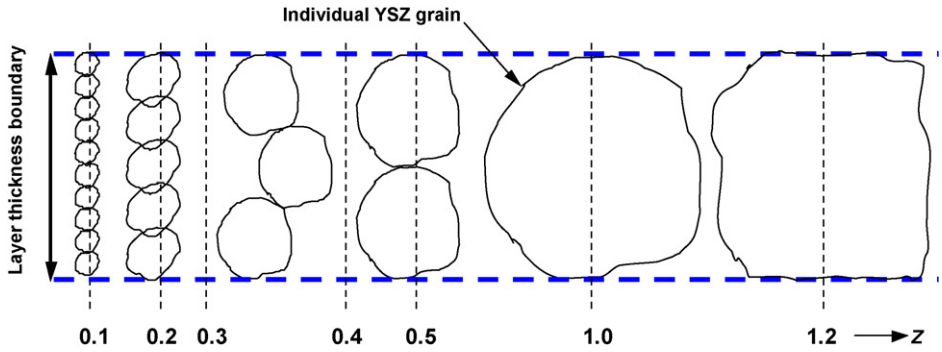

Fig. 8. Schematic diagram illustrating the mean grain size to sintered layer thickness factor, z. The factor increases to 1 as the grain size becomes equal to the sintered layer thickness.

the surface grain size becomes greater than the thickness of the sintered layer, z becomes greater than 1.

The effect of gas permeance is plotted as a function of z and the results are shown in Fig. 9. At a z factor value between approximately 0.1 and 0.3 the gas permeance is at a minimum. This corresponds to the 165 and 200 mesh sizes with a gas permeance of $1.30 \times 10^{-4} \pm 2.0 \times 10^{-5}$ and $1.3 \times 10^{-4} \pm 3.3 \times 10^{-6}$ mbar l s^{-1} cm^{-2}, respectively. Where the z factor is <0.1 or >0.3 there is an increase in gas permeance up to a maximum value of $2.7 \times 10^{-4} \pm 7.4 \times 10^{-6}$ mbar l s^{-1} cm^{-2} for the 325 mesh size. The highest gas permeance corresponds to a z factor where there are less than two grains across the sintered layer thickness. Thus, if there are too many or too few grains relative to the sintered layer thickness there is an increase in gas permeance. Hence the grain size and sintered thickness are potentially more useful parameters to measure than the degree of densification when assessing the gas permeance of thick-film layers. Further investigation would be required to assess the validity of this approach over a wider range of processing parameters.

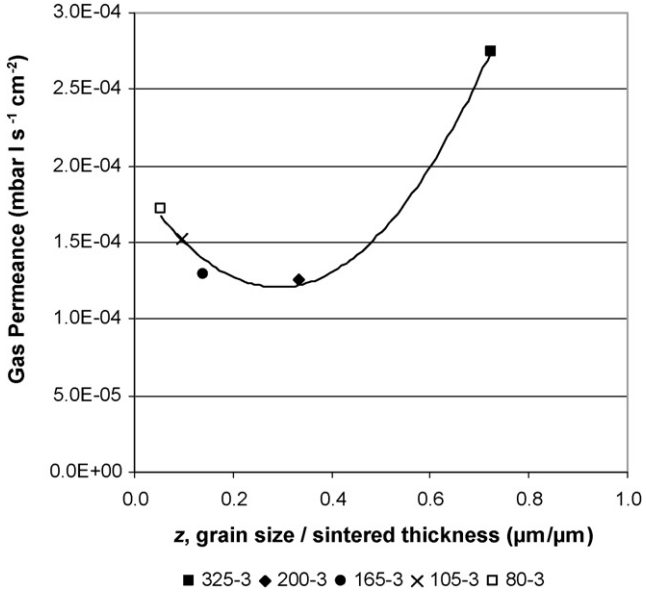

Fig. 9. Gas permeance as a function of the ratio of grain size to sintered layer thickness.

4. Conclusions

Experiments have been conducted on the screen-printing of micrometre sized 3 mol% YSZ thick-film layers on pre-fired substrates. A change of mesh size results in a change in the deposited and sintered layer thickness. This change in layer thickness causes an associated change in the microstructure of the sintered layers. Increasing screen thickness leads to a thicker sintered layer, a reduction in relative density and a reduction in grain size. However, the thinnest, most dense layer did not have the lowest gas permeance, possibly because the grain size to thickness ratio was too low. An optimum mesh size allowed the fabrication of 9 ± 0.8 μm thick layers having a gas permeance of 1.3×10^{-4} mbar l s^{-1} cm^{-2}. Therefore, it was concluded that the screen thickness is the major factor influencing relative density, grain size and consequently gas permeance of screen-printed zirconia layers.

Acknowledgements

The authors would like to acknowledge Dr Graeme Roberts (MCS, Midlothian, UK) for performing the SEM analysis and calibrating the SEM sufficiently to meet the ASTM standard and Rolls-Royce Fuel Cell Systems Limited for their support with the gas testing.

References

1. Laberty, R. C., Ansart, F., Deloget, C., Gaudon, M. and Rousset, A., Dense yttria zirconia: sintering and microstructure. *Ceram. Int.*, 2003, **29**, 151–158.
2. Minh, N. Q., Ceramic fuel cells. *J. Am. Ceram. Soc.*, 1993, **76**(3), 563–588.
3. Singhal, S., Advances in solid oxide fuel cell technology. *Solid State Ionics*, 2000, **135**(1–4), 305–313.
4. Gardner, F. J., Day, M. J., Brandon, N. P., Pashley, M. N. and Cassidy, M., SOFC technology development at Rolls-Royce. *J. Power Sources*, 2000(86), 122–129.
5. Barnett, S. A., A new solid oxide fuel-cell design based on thin-film electrolytes. *Energy*, 1990, **15**(1), 1–9.
6. Chen, Y.-Y. and Wei, W.-C. J., Processing and characterization of ultra-thin yttria-stabilized zirconia (YSZ) electrolytic films for SOFC. *Solid State Ionics*, 2006, **177**, 351–357.
7. Maskell, W. C., Progress in the development of zirconia gas sensors. *Solid State Ionics*, 2000, **134**, 43–50.
8. Debeda-Hickel, H., Lucat, C. and Menil, F., Influence of the densification parameters on screen-printed component properties. *J. Eur. Ceram. Soc.*, 2005, **25**, 2115–2119.

9. Bordia, R. K. and Scherer, G. W., On constrained sintering. I. Constitutive model for a sintering body. II. Comparison of constitutive models. III. Rigid inclusions. *Acta Metall.*, 1988, **36**(9), 2393–2416.
10. Mochizuki, K., Sorita, R., Takashima, H., Nakamura, K. and Lu, G., Sensing characteristics of a zirconia-based CO sensor made by thick-film lamination. *Sens. Actuators B*, 2001, **77**, 190–195.
11. Zhang, Y., Huang, X., Lu, Z., Liu, Z., Ge, X., Xu, J., Xin, X., Sha, X. and Su, W., A study of the process for yttria-stabilized zirconia electrolyte films prepared by screen-printing. *J. Power Sources*, 2006, **160**, 1065–1073.
12. Gaudon, M., Menzler, N. H., Djurado, E. and Buchkremer, H. P., YSZ electrolyte of anode-supported SOFCs prepared from sub micron YSZ powders. *J. Mater. Sci.*, 2005, **40**(14), 3735–3743.
13. Park, Y. I., Cha, S. W., Saito, Y. and Prinz, F. B., Gas-tight alumina films on nanoporous substrates through oxidation of sputtered metal films. *Thin solid films*, 2005, **476**, 168–173.
14. Hinton, P. R., *Statistics Explained* (*2nd ed.*). East Sussex, Routledge, Hove, 2004, pp. 369.
15. Maca, K. and Siminikova, S., Effect of sintering schedule on grain size of oxide ceramics. *J. Mater. Sci.*, 2005, **40**, 5581–5589.